SANDIA REPORT

SAND2003-8230
Unlimited Release
Printed May 2003

Finite Element Thermal Analysis of 155-mm Projectile Exudtion Inside a Hot Gun Tube

T. R. Shelton, Y. R. Kan

Prepared by
Sandia National Laboratories
Albuquerque, New Mexico 87185 and Livermore, California 94550

Sandia is a multiprogram laboratory operated by Sandia Corporation,
a Lockheed Martin Company, for the United States Department of Energy's
National Nuclear Security Administration under Contract DE-AC04-94AL85000.

Sandia National Laboratories

Issued by Sandia National Laboratories, operated for the United States Department of Energy by Sandia Corporation.

Available to DOE and DOE contractors from
U.S. Department of Energy
Office of Scientific and Technical Information
P.O. Box 62
Oak Ridge, TN 37831

Telephone: (865)576-8401
Facsimile: (865)576-5728
E-Mail: reports@adonis.osti.gov
Online ordering: http://www.doe.gov/bridge

Available to the public from
U.S. Department of Commerce
National Technical Information Service
5285 Port Royal Rd
Springfield, VA 22161

Telephone: (800)553-6847
Facsimile: (703)605-6900
E-Mail: orders@ntis.fedworld.gov
Online order: http://www.ntis.gov/help/ordermethods.asp?loc=7-4-0#online

SAND 2003-8230
Unlimited Release
Printed May 2003

Finite Element Thermal Analysis of 155-mm Projectile Exudation Inside a Hot Gun Tube

T. R. Shelton and Y.R. Kan
Engineering Mechanics Modeling & Simulation Department
Sandia National Laboratories
Livermore, California 94551-0969

Abstract

The high firing rates of new and developing cannons create higher operating temperatures that projectiles experience. Higher temperatures in-bore bring the possibility of high explosive exudation from chambered shells during misfire, hang-fire, or hold-fire. The development of a finite element thermal model to predict high explosive exudation inside a hot gun tube brings an improved level of insight to existing physical test results. The M198 towed howitzer and M107 155-mm shell are modeled to compare to physical test results from Morales 1997 and Zimmerman 1980. During creation of the model special focus is taken to simulate the heat flow between the contact of the rotating band and cannon wall. A strong correlation between test results and model is seen with both reports and validates the model setup. Model results suggest that time to exudation predicted by Morales and Zimmerman may be too conservative.

ACKNOWLEDGEMENT

Special thanks goes to Tim Dacier and Kok Chung of ARDEC for technical guidance, Yuki Ohashi (8727 Engineering Mechanics Modeling & Simulation Department) for thermal analysis support and Carmella Orham (8727 Engineering Mechanics Modeling & Simulation Department) for help on formatting and presentation of results.

CONTENTS

LIST OF FIGURES

No.

LIST OF EQUATIONS

No.

Finite Element Thermal Analysis of 155-mm Projectile Exudation Inside a Hot Gun Tube

1.0 Introduction

As the army demands artillery guns with higher firing rates, increasing from two to three rounds per minute up to ten rounds per minute, operating temperatures of the bores on tanks and howitzers increase comparatively. In the course of normal operation, a chambered shell does not remain chambered long enough to be affected by the raise in operating temperature. However, if a misfire, hang-fire, or hold-fire occurs then the chambered shell begins to rise in temperature approaching the melting temperature of its incased explosive. If the explosive melts it has the potential to escape through the fuze and into the bore. The escaping of melted explosives is termed "exudation". Exudation generates an in-bore detonation hazard. Predicting when exudation occurs is a vital part to setting a standard for safe-time-to-fire. The safe-time-to-fire tells the operator how long they have to un-chamber/fire the loaded round before they need to evacuate the mount/tank. Earlier tests have been performed to establish the existing safe-time-to-fire and it is the objective of this study to expand and improve on these tests through the use of a finite element thermal model.

2.0 Related Studies

The concern about weapon exudation is not a new topic. Since the Navy started firing at high rates sooner, they have been examining exudation and gun barrel temperature related problems since as early as 1953 [1]. Zimmermann and Geanny performed one of the earliest tests in 1980 that relates to safe-time-to-fire for the army [2]. The M198 towed howitzer had recently been developed with a TWD (Thermal Warning Device) and Zimmermann and Geanny were attempting to use readings from the TWD to more accurately predict exudation of M107 and M549 155-mm rounds. Zimmermann and Geanny concluded the safe-time-to-fire should be reduced from the accepted 10 min. when the TWD temperature reads 350 °F. Following the Zimmerman study, thermal testing was again performed on the M198 towed howitzer. Testing in 1997 by Morales concluded the safe-time-to-fire should be reduced even further than Zimmerman's suggested time [3]. To better understand exudation and the reasons for different findings in the two tests, a thermal finite element model can be very useful.

3.0 Building A FE Model

The expected primary heat transfer we are trying to capture flows from the hot cannon wall into the round by means of conduction. The magnitude of convection and radiation heating the round are small enough relative to the expected conduction that they can be ignored in creating the model. For this model, the most complicated aspect is all the material interfaces (Figure 1). To aid in capturing the heat flow between these materials, the mesh size is kept relatively small around the interfaces (Figure 2).

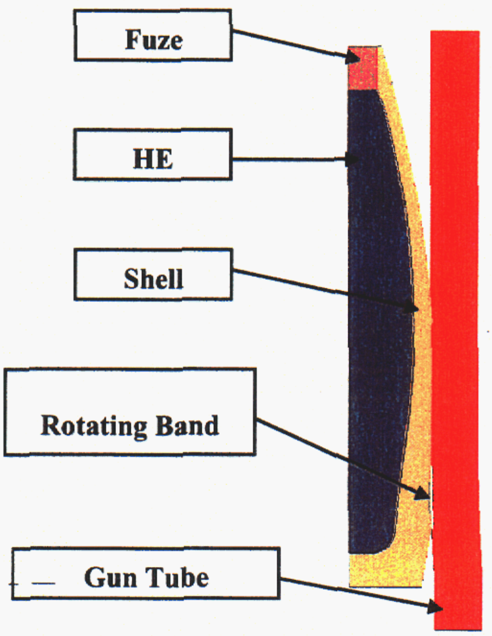

Figure 1: Material interfaces.

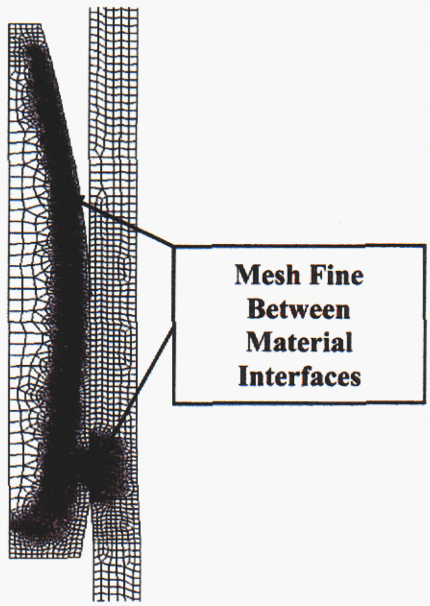

Figure 2: Mesh detail at material interfaces.

Looking at the material properties, it is important to note the differences in the conductivities (Figure 3). Comparing the different conductivities of all the materials further emphasizes the need to capture interface interactions because the rotating band has four times the conductivity of steel and steel has one hundred and fifty times the conductivity of the explosives.

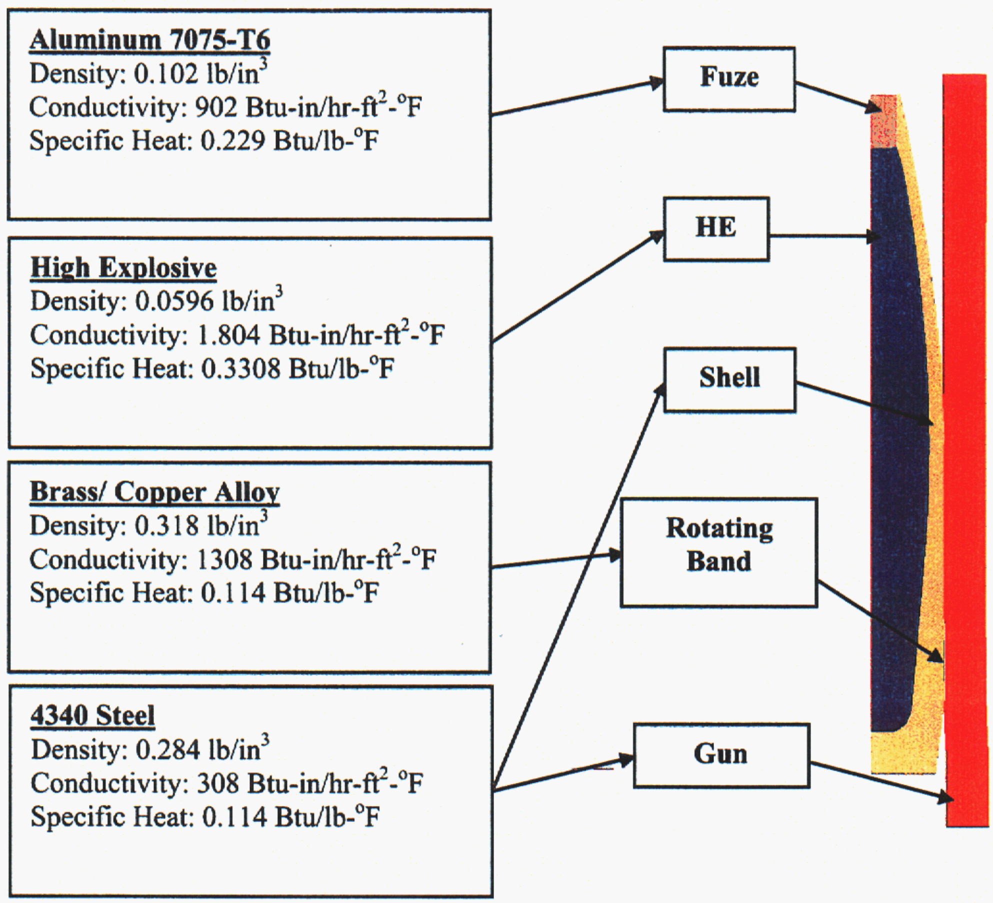

Figure 3: Material properties.

An approximation is needed to model the conductance between the rotating band and the cannon wall. All the other interfaces in the round are easily approximated as welds or perfect conductance between materials.

A small surface in the model was made so its conductivity could be adjusted to simulate the contact interface of the rotating band and cannon wall seen in Figure 4.

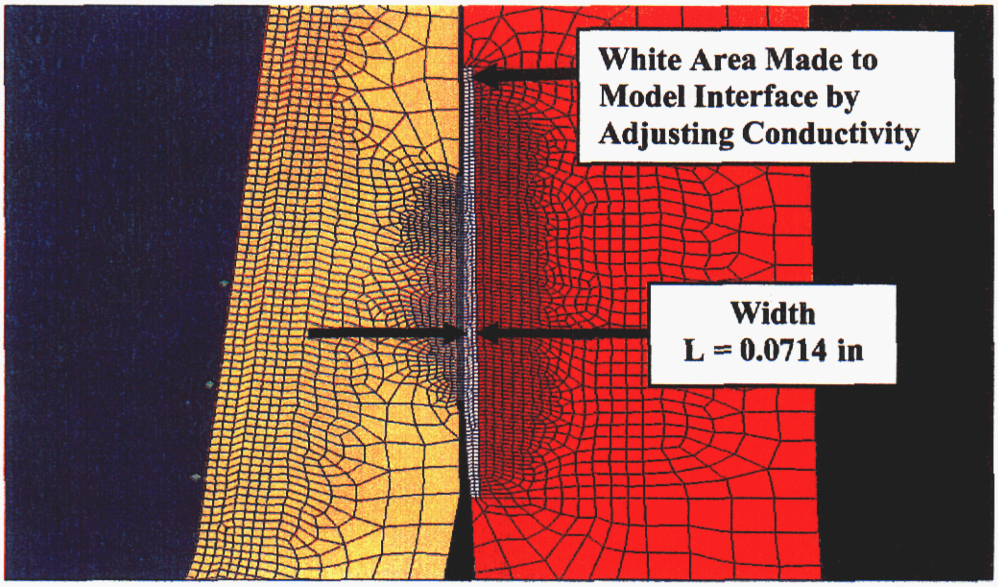

Figure 4: Surface for interface conductance approximation.

Using the formula [1] below from a report generated by Yuki Ohashi, a linear approximation of the effective interface conductivity was determined for the white area.

[1] $$K_{ef} = \frac{(k \cdot h_i \cdot L)}{(h_i \cdot L + k)}$$

L in the formula stands for the width of the adjusted material, k stands for the current conductivity of the material which is going to be adjusted. In this case $L = 0.0714\ \text{in}$ and k is that of steel, $k = 308 \frac{\text{Btu} \cdot \text{in}}{\text{hr} \cdot \text{ft}^2 \cdot {}^\circ\text{F}}$. The variable h_i, interface conductance, is determined by referring to the Handbook of Heat Transfer. Figure 5 shows a table and plot taken from the Handbook of Heat Transfer. Assuming an initial contact pressure of 50 psi and using curve 15, because it corresponds to a copper interface, gets a value for $h_i = 1400 \frac{\text{Btu}}{\text{hr} \cdot \text{ft}^2 \cdot {}^\circ\text{F}}$. The interface conductance can be assumed to remain constant even though the contact pressure will increase due to thermal expansion. The assumption of a constant interface conductance is valid because of the horizontal nature of curve 15 for copper, which implies changes in pressure bring about very little change in the interface conductance.

3-16 Handbook of Heat Transfer

TABLE 1. Interface Conditions for Conductance Data in Fig. 8

Curve	Material pair	RMS surface finish (μ in.)	Gap material	Mean contact temp. (°F)	Ref.
1	aluminum (2024-T3)	48–65	vacuum (10^{-4} mm Hg)	110	5
2	aluminum (2024-T3)	8–18	vacuum (10^{-4} mm Hg)	110	5
3	aluminum (2024-T3)	6–8 (not flat)	vacuum (10^{-4} mm Hg)	110	5
4	aluminum (75S-T6)	120	air	200	6
5	aluminum (75S-T6)	65	air	200	6
6	aluminum (75S-T6)	10	air	200	6
7	aluminum (2024-T3)	6–8 (not flat)	lead foil (0.008 in.)	110	5
8	aluminum (75S-T6)	120	brass foil (0.001 in.)	200	6
9	stainless (304)	42–60	vacuum (10^{-4} mm Hg)	85	7
10	stainless (304)	10–15	vacuum (10^{-4} mm Hg)	85	7
11	stainless (416)	100	air	200	6
12	stainless (416)	100	brass foil (0.001 in.)	200	6
13	magnesium (AZ-31B)	50–60 (oxidized)	vacuum (10^{-4} mm Hg)	85	7
14	magnesium (AZ-31B)	8–16 (oxidized)	vacuum (10^{-4} mm Hg)	85	7
→15	copper (OFHC)	7–9	vacuum (10^{-4} mm Hg)	115	7
16	stainless/aluminum	30/65	air	200	6
17	iron/aluminum	—	air	80	8
18	tungsten/graphite	—	air	270	8

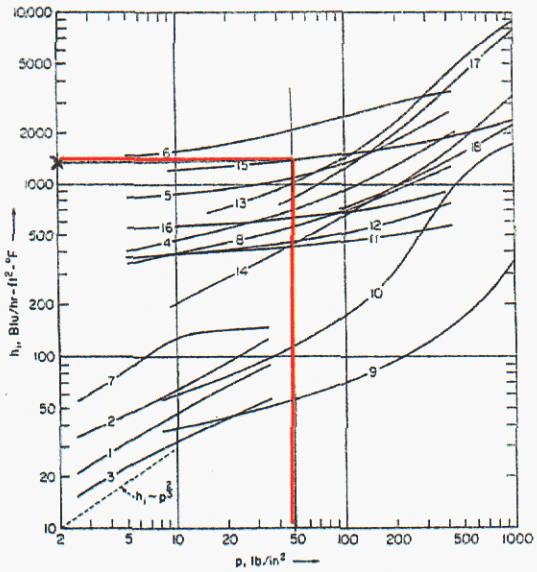

Fig. 8. Thermal interface conductance data.

Figure 5: Table and figure from Handbook of Heat Transfer used in determining the interface conductance.

Before combining all the variables to calculate the effective conductivity, it is also necessary to adjust the effective conductivity for the percentage of contact it actually makes with the barrel. The rotating band sits in the rifling shown in Figure 6.

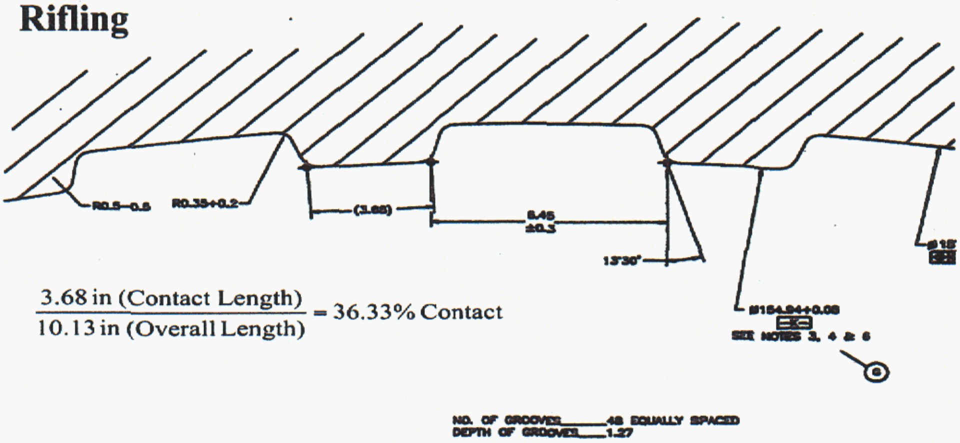

Figure 6: Rifling of cannon determines contact percentage with rotating band.

Taking the contact percentage, 36.33%, and the other variables into consideration yield an effective conductivity, $K_{ef} = 27.43 \frac{\text{Btu} \cdot \text{in}}{\text{hr} \cdot \text{ft}^2 \cdot {}^\circ\text{F}}$. This new conductivity for the white area in Figure 4 comes out to be about 9% of its original conductivity. Having materials, geometry, mesh, and interface conditions defined the model is ready to start simulating varying initial conditions.

4.0 Validating Model Setup and Simulation by Comparison to Physical Testing

To compare with the testing performed by Morales in 1997, temperature data collected by thermocouples was compared to nodal data in the simulation model. Figure 7 shows a diagram of the instrumented round along side the model to point out the comparison of thermocouple 17 to node 5950.

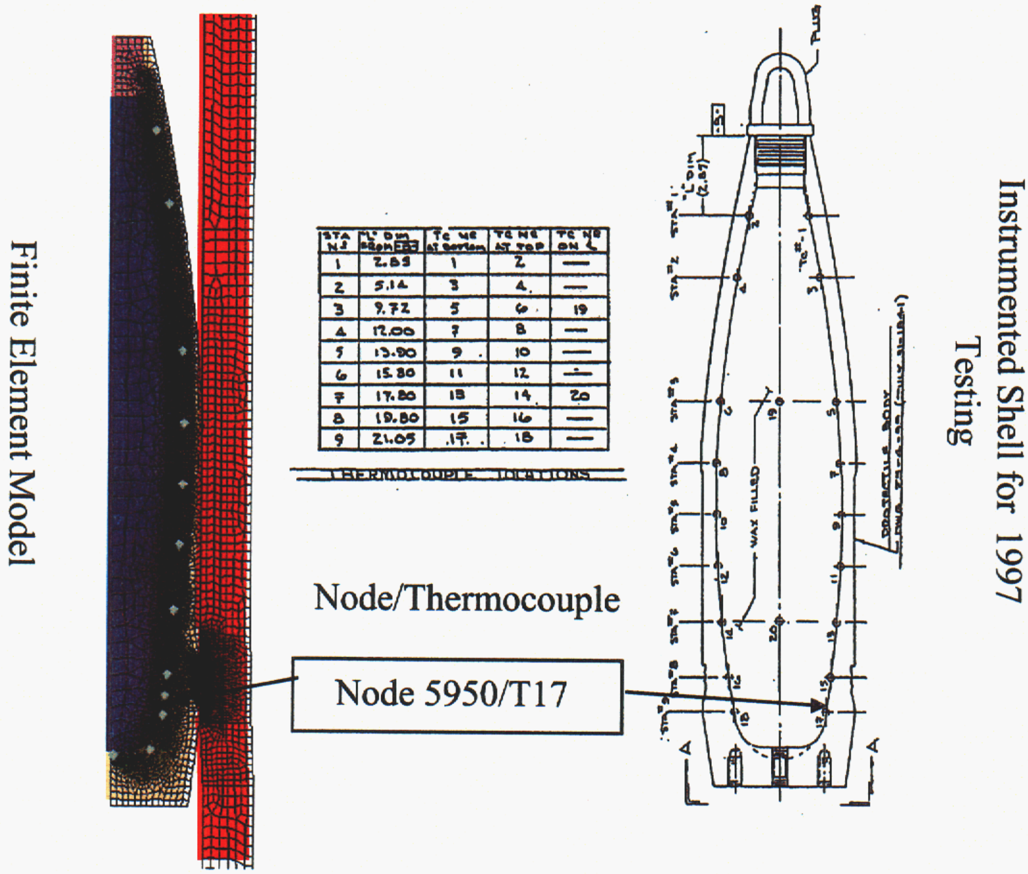

STA NO	'L' DIM FROM [illegible]	TC NO AT BOTTOM	TC NO AT TOP	TC NO ON ℄
1	2.83	1	2	—
2	5.14	3	4	—
3	9.72	5	6	19
4	12.00	7	8	—
5	13.90	9	10	—
6	15.80	11	12	—
7	17.80	13	14	20
8	19.80	15	16	—
9	21.05	17	18	—

Figure 7: Model setup compared to 1997 Morales test setup.

The thermocouple 17 was chosen to compare to since it obtains the maximum temperature during the testing. The comparison between the thermocouple and node can be seen in Figure 8.

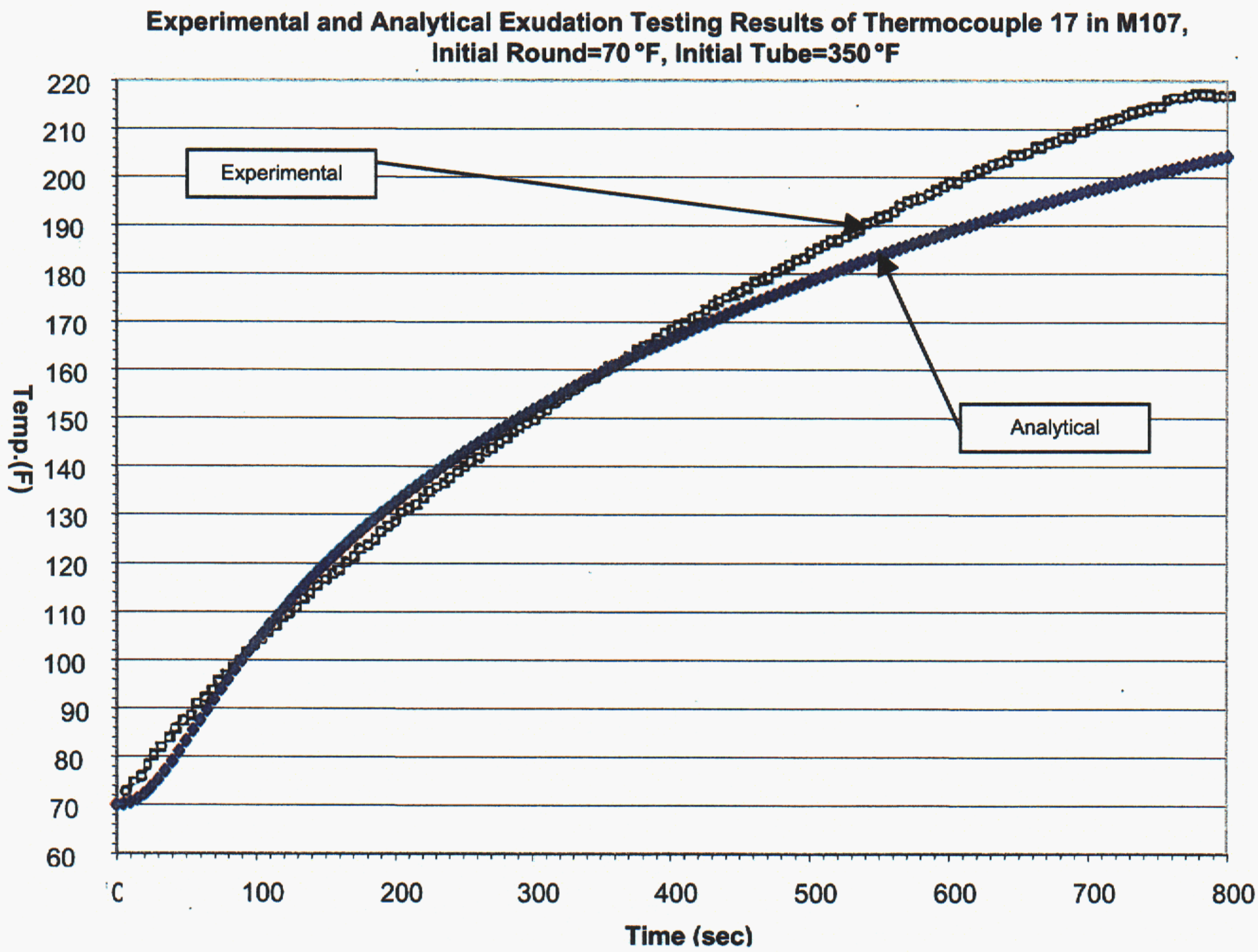

Figure 8: Thermocouple to Node data comparison for 1997 Morales Testing.

The data remains very close all the way through the melt temperature of the high explosives.

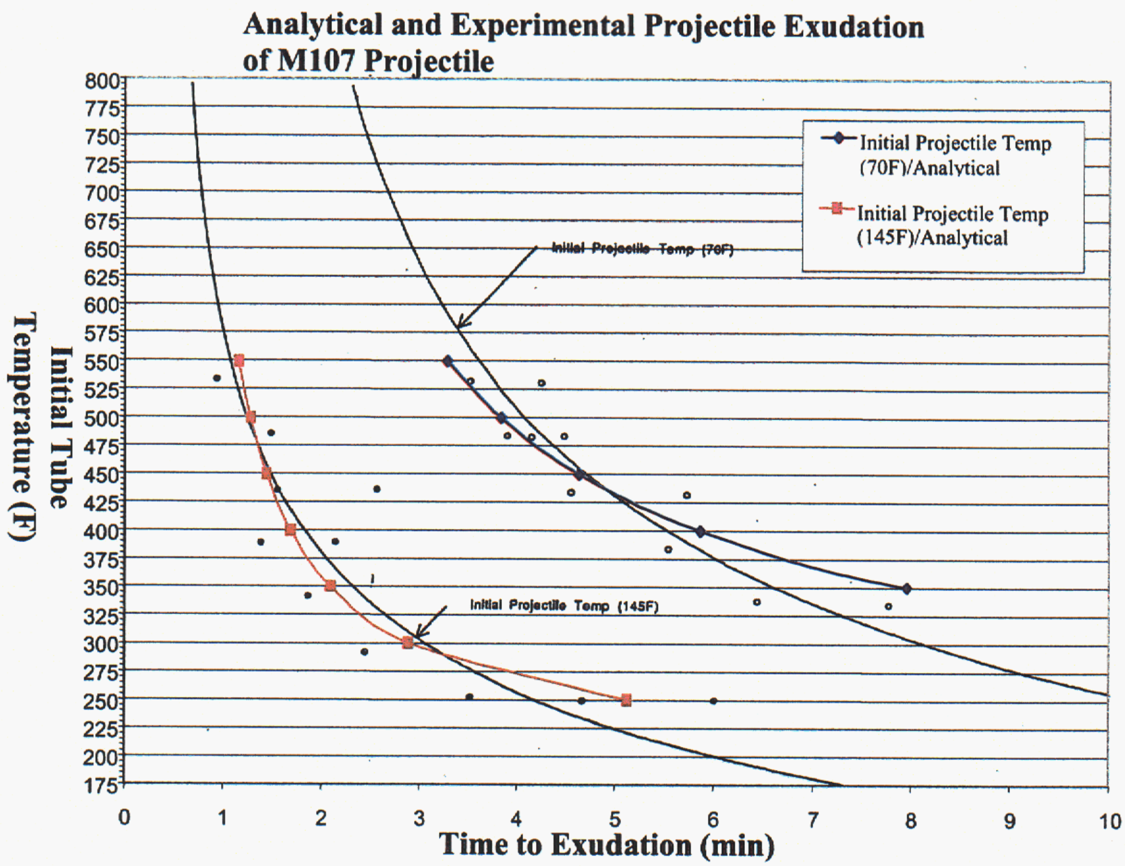

Figure 9: Time to exudation results of 1997 Morales testing compared to analytical predictions.

The most comprehensive plot that collects data from multiple tests was chosen for comparison. Experimental data plotted in Figure 9 was gained by placing a round at 70 °F or 145 ° F into a cannon at an initial temperature ranging from 550 °F to 250 °F and waiting for any of the thermocouples to reach 176 °F and recording this time. 176 °F is the melt temperature of HE. The time it takes a thermocouple to reach 176 °F is considered the time to exudation. The analytical data plotted was obtained by letting a simulation with similar initial temperatures run until node 5950 reached the melt temperature of 176 °F. The analytical data compares very well with the experimental data closely predicting the same time to exudation.

A comparison to testing performed by Zimmermann and Geany in 1981 is done in a similar manner as was done with the 1997 testing by Morales. Again, a thermocouple to node reading was used. The test setup compared to model setup for the 1981 test can be seen in Figure 10.

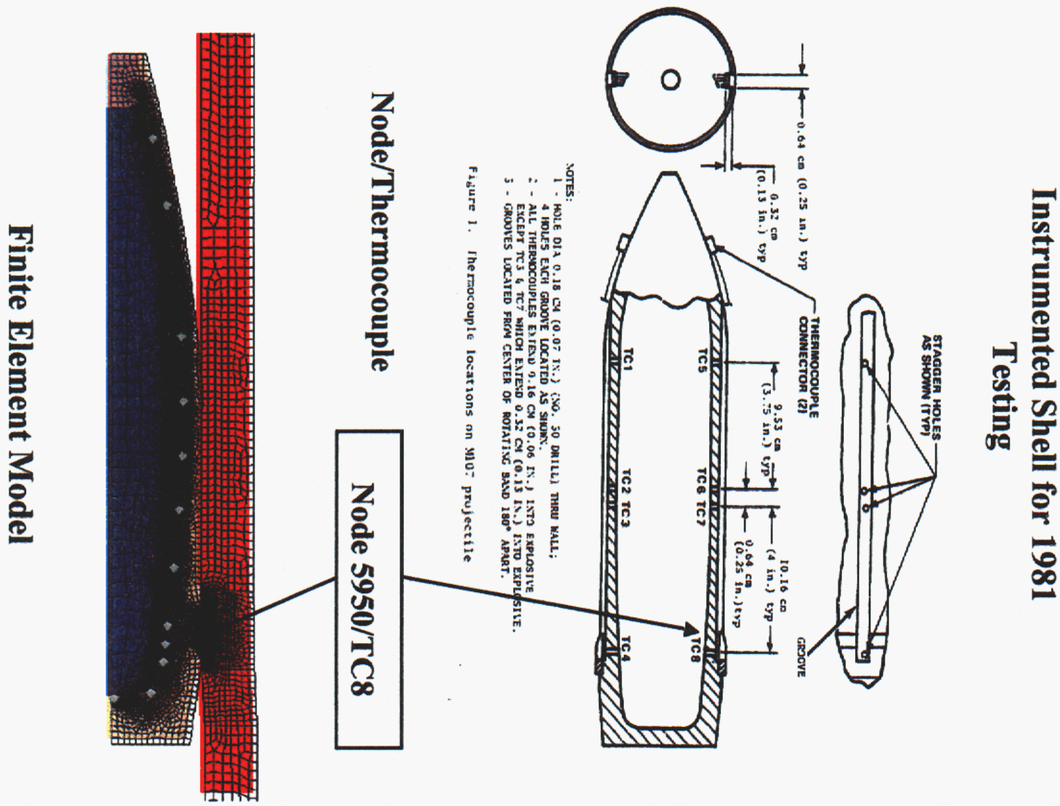

Figure 10: Model setup compared to 1981 Zimmermann and Geany test setup.

The data from the 1981 tests was not compiled in the same manner as the 1997 tests. Instead, individual thermocouple temperature readings versus time plots were made for shells loaded at varying initial temperatures and into a cannon at varying temperature. Thermocouple data from several of the tests are plotted with the node temperature data with the same conditions in the following figures. The analytical results follow the same trend as the experimental results while slightly over predicting the temperature. The over predicting of the temperature can be explained by the test setup for the experiment. Since thermocouples were placed by drilling into the shell, removing of the material in front of the thermocouple would block heat flow to the thermocouple. Good correlation to both the 1981 and 1997 testing helps validate the model setup and output.

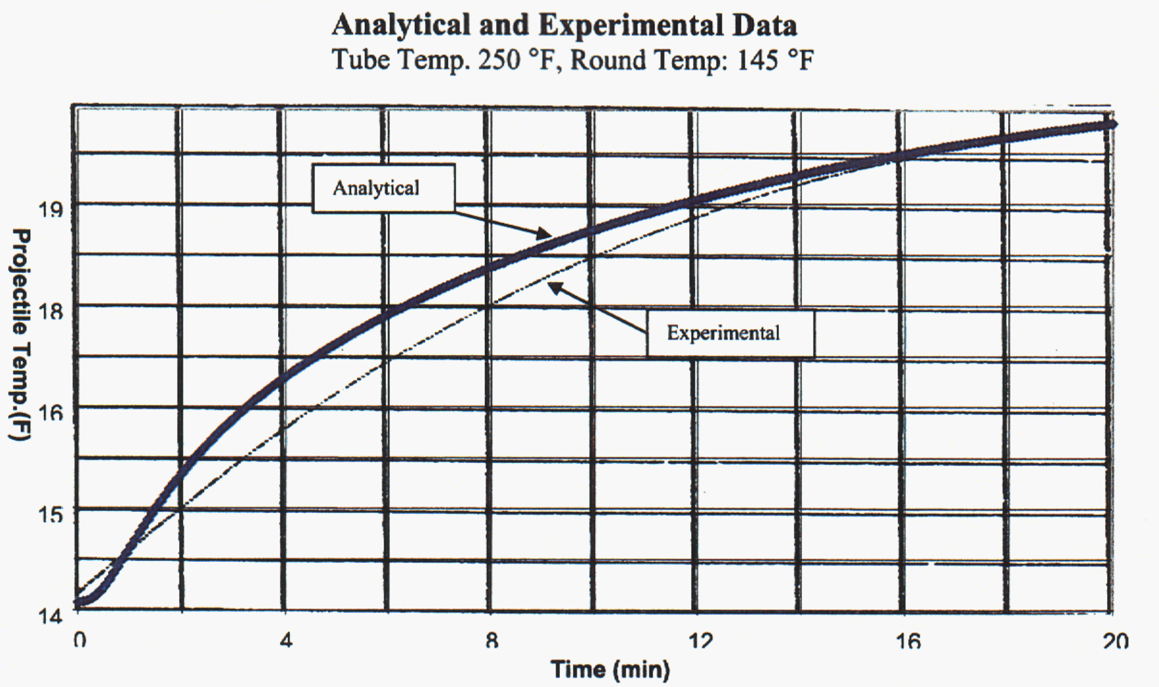

Figure 11: Thermocouple temperature versus time from 1981 testing compared with analytical prediction. Initial tube temperature of 250 °F and initial round temperature of 145 °F.

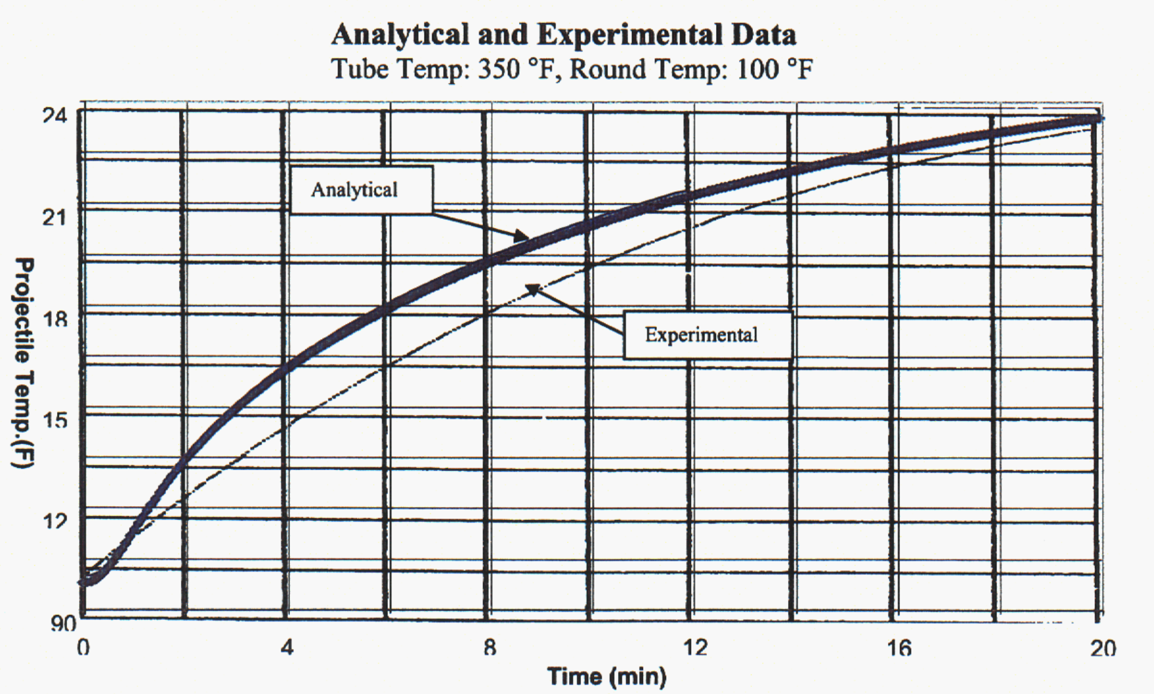

Figure 12: Thermocouple temperature versus time from 1981 testing compared with analytical prediction. Initial tube temperature of 350 °F and initial round temperature of 100 °F.

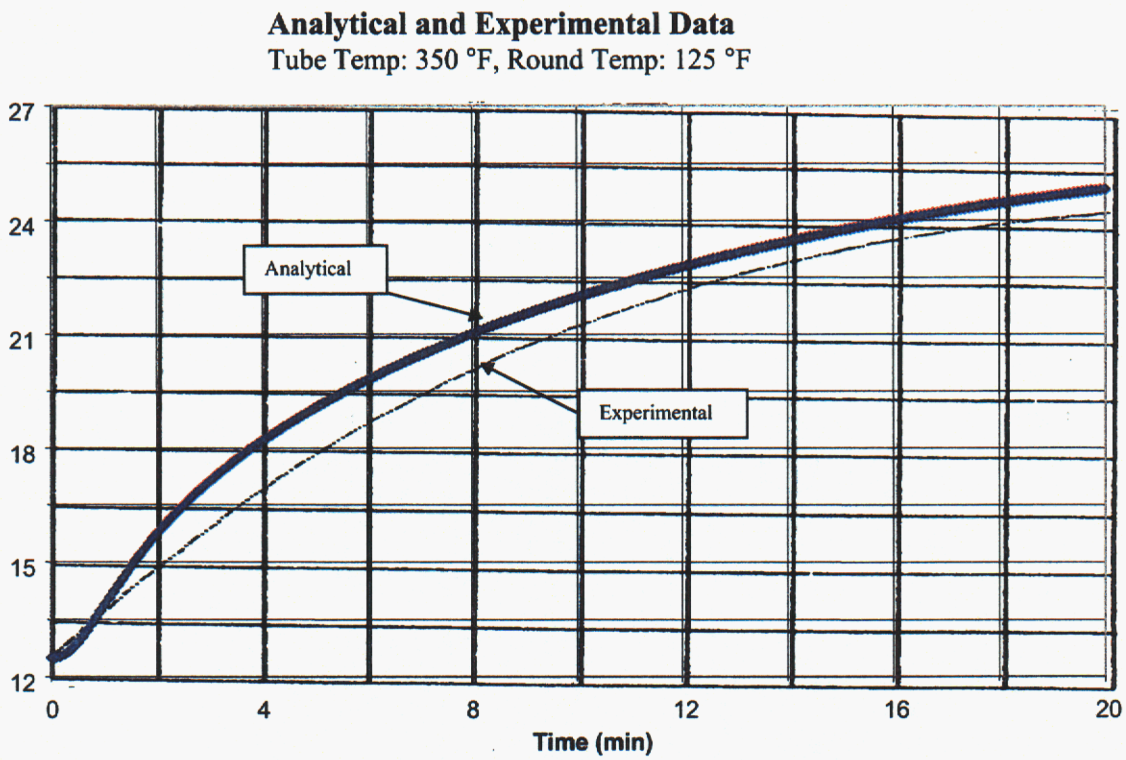

Figure 13: Thermocouple temperature versus time from 1981 testing compared with analytical prediction. Initial tube temperature of 350 °F and initial round temperature of 125 °F.

5.0 Insight from Model Visualization

One of the strengths of finite element models is the their ability to aide in visualizing results. In thermal analysis an infrared picture is one of the best ways to see heat bands.

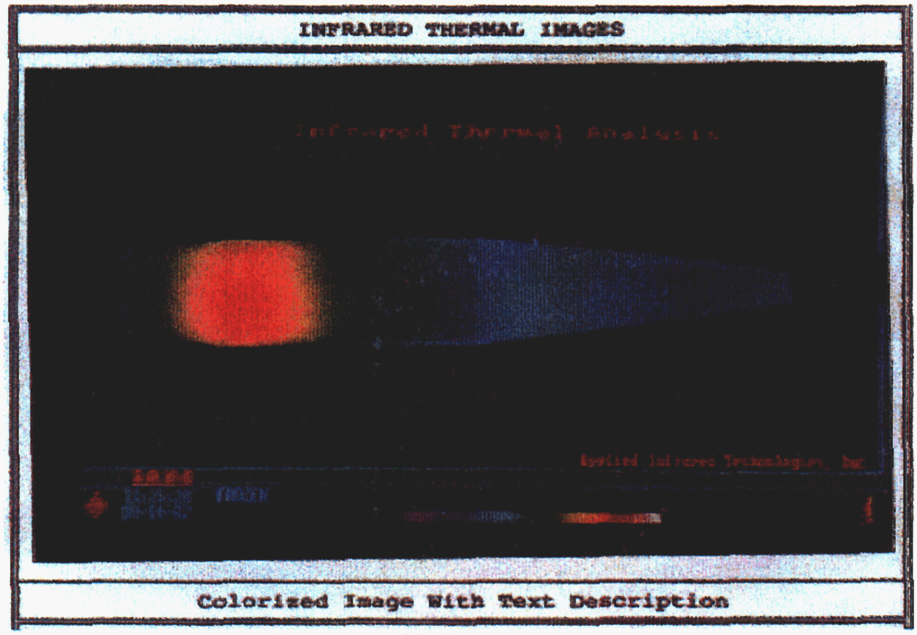

Figure 14: Infrared image of M107 projectile from testing done by Benet Laboratories.

Evidence that all the heat flow from the cannon comes through the rotating band was demonstrated by a thermal image captured in testing by Benet Laboratories (Figure 14). A M107 projectile was loaded and then unloaded and photographed when the rotating band reached 176 °F. The picture clearly indicates all the heat is absorbed in through the rotating band. A thermal contour plot of the shell and rotating band from the finite element model shows comparable heat bands (Figure 15).

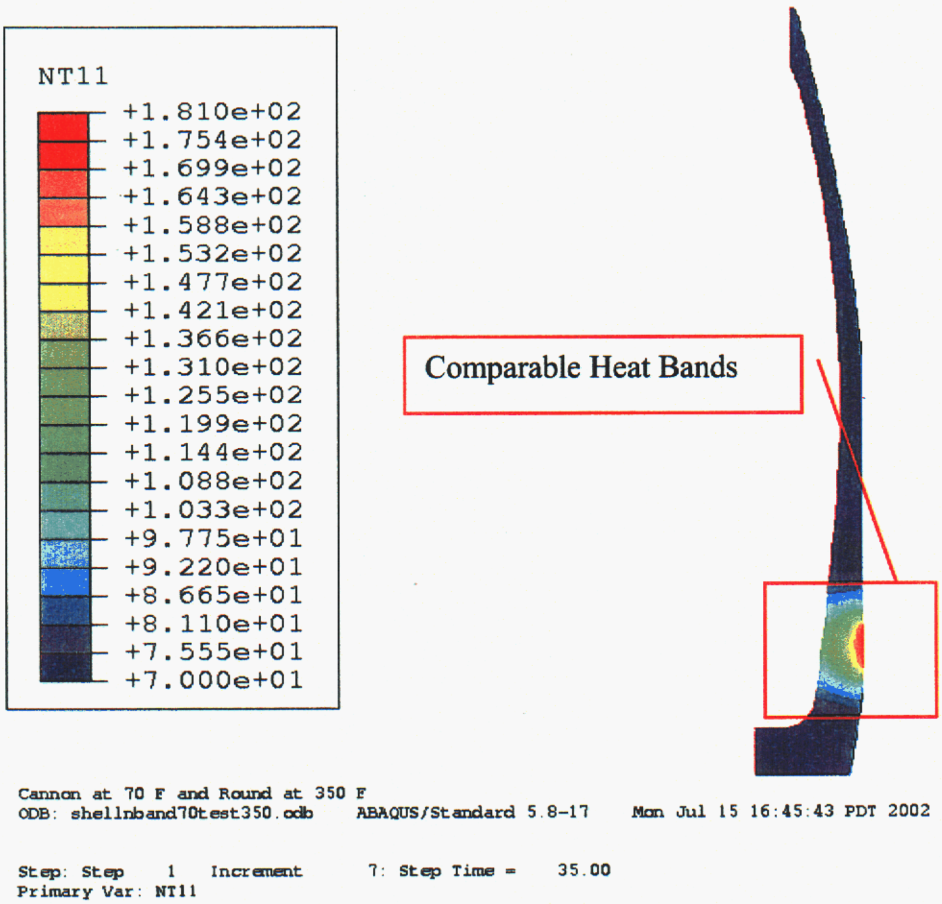

Figure 15: Finite element model thermal contours illustrate comparable heat bands to the infrared image.

Also, an overall contour plot of the model correctly shows the model pulling heat from the gun tube into the shell (Figure 16). Using the finite element model to focus on the high explosives at the time predicted as melt shows a very thin layer, which is at or above the melt temperature (Figure 17 & Figure 18). This thin layer of melt may not be enough to actually cause exudation.

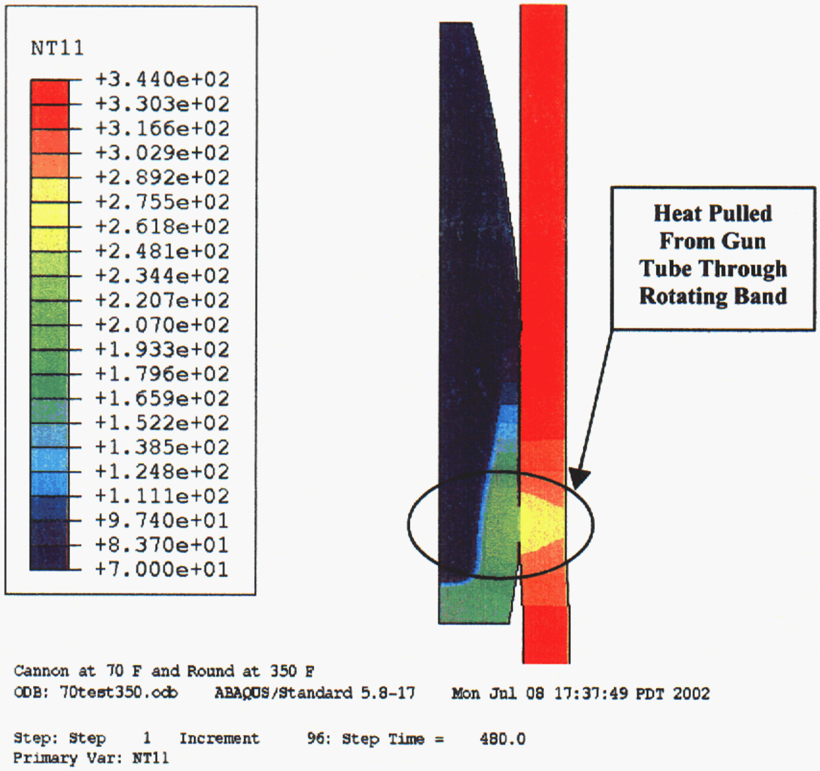

Figure 16: Finite element model thermal contours illustrate heat flow from gun tube to round through rotating band.

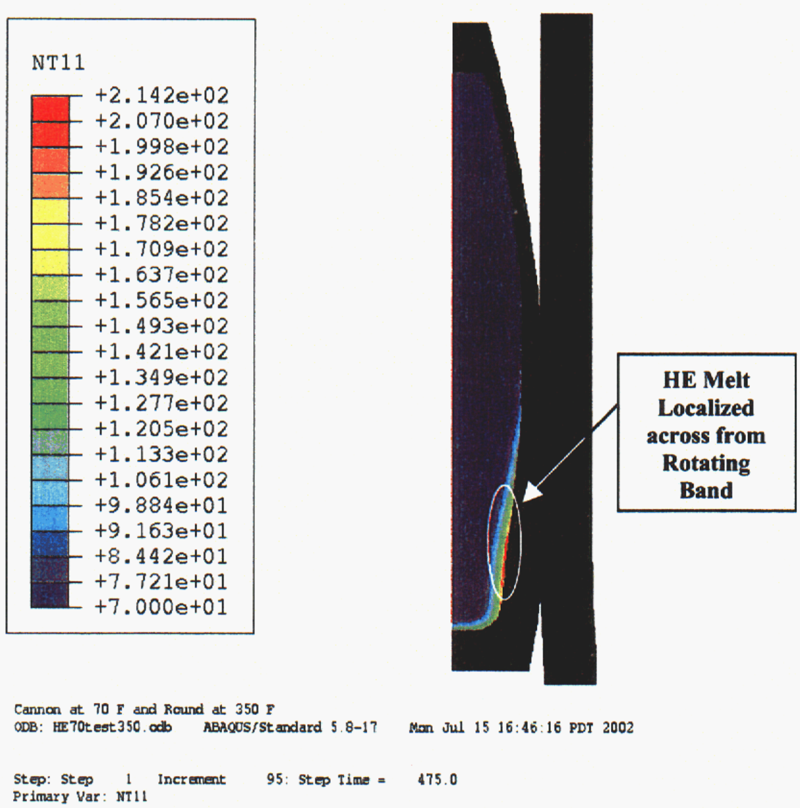

Figure 17: Thin layer of melt temperatures in high explosives seen in model at time predicted for exudation.

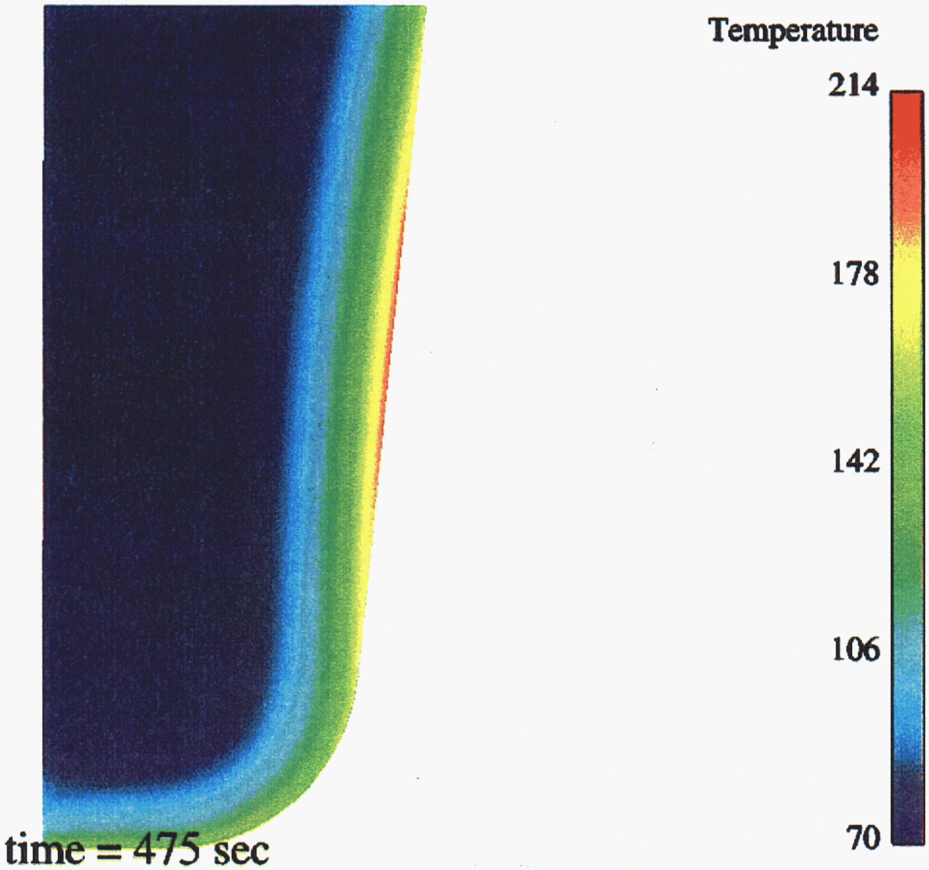

Figure 18: Zoomed in picture of thin layer of melt temperatures in high explosives seen in model at time predicted for exudation.

6.0 Conclusions

An accurate finite-element thermal analysis model has been developed to predict the heating of a seated projectile. The model correlates to results produced by experiments in 1997 by Morales and 1981 by Zimmerman and Geany. Also, the model brings insight to the depth of melt, which may prove the safe-time-to-fire predicted by Morales and Zimmerman to be too conservative. A thin layer melt may not be a concern for exudation, but when the melting propagates to the entire backend then it poses an in-bore safety risk from torsional impulse loading. This model can be used for further study into the thickness of the melting zone. Finally, this approach can be extended to model various munitions and gun systems.

7.0 References

1. Macatician and Nanigian. “A Thermocouple to Record Transient Temperatures at the Bore Surface of Guns.” 1953, NPG Report 1130, Dahgren, Virginia

2. Geany, Ronald G. and John R. Zimmerman. “Temperature Corerelation for Heated M198 Towed Howitzer Gun Tube and Chambered 155-MM Projectile.” 1981, ARTSD-TR-80004, Dover, New Jersey

3. Ciro A. Morales III. “Thermal Effects of a Hot Weapon on High Explosive Projectiles.” 1997, ARCCB-TR-97024, Watervliet, New York

Distribution

1 Commander
U.S. Army Research Development, and Engineering Center
Attn: AMSTA-AR-FSA, Michael Chiefa
Picatinny Arsenal, NJ 07806-5000

1 Commander
U.S. Army Research Development, and Engineering Center
Attn: AMSTA-AR-P, Kok Chung
Picatinny Arsenal, NJ 07806-5000

1 Commander
U.S. Army Research Development, and Engineering Center
Attn: AMSTA-AR-P, Dominic Demella
Picatinny Arsenal, NJ 07806-5000

1 Commander
U.S. Army Research Development, and Engineering Center
Attn: AMSTA-AR-P, Bob Lee
Picatinny Arsenal, NJ 07806-5000

1 Commander
U.S. Army Research Development, and Engineering Center
Attn: AMSTA-AR-SSA-S, Tim Dacier
Picatinny Arsenal, NJ 07806-5000

1 Commander
U.S. Army Research Development, and Engineering Center
Attn: AMSTA-AR-SSA-S, Lee Mund
Picatinny Arsenal, NJ 07806-5000

1 Commander
U.S. Army Research Development, and Engineering Center
Attn: AMSTA-AR-SSA-S, Susan Traendly
Picatinny Arsenal, NJ 07806-5000

1 Commander
U.S. Army Research Development, and Engineering Center
Attn: Project Manager, Office for Advanced Field Artillery Systems, OPM-AFAS
Picatinny Arsenal, NJ 07806-5000

1 U.S. Army Research Laboratory
Attn: AMSRL-WM-WB, Jonathan Montgomery
Watertown Site
Whitetown, MA 02172

1		U.S. Army Research Laboratory Attn: AMSRL-WM-T. Bruce Burns Aberdeen Proving Ground, MD 21005-5066
1		U.S. Army Research Laboratory Attn: AMSRL-WM-WB, Jim Bender Aberdeen Proving Ground, MD 21005-5066
1		U.S. Army Research Laboratory Attn: AMSRL-WM-WB, William Drysdale Aberdeen Proving Ground, MD 21005-5066
1		U.S. Army Research Laboratory Attn: AMSRL-WM-WB, Al Horst Aberdeen Proving Ground, MD 21005-5066
1	MS 9001	M. E. John, 8000 Attn: R. H. Stulen, 8100, MS 9004 D. R. Henson, 8200, MS 9007 W. J. McLean, 8300, MS 9054 P. N. Smith, 8500, MS 9002 K. E. Washington, 8900, MS 9003
1	MS 9035	W. G. Wilson, 8230
10	MS 9042	Y-R. Kan, 8727
1	MS 9042	Y. Ohashi, 8727
1	MS 9042	A. R. Ortega, 8727
5	MS 9042	T. R. Shelton, 8727
1	MS 9042	P. A. Spence, 8727
1	MS 9402	K. L. Wilson, 8703 Attn: J. C. F. Wang, 8723, MS 9403 C. H. Cadden, 8724, MS 9402 E-P Chen, 8726, MS 9161
1	MS 9402	W. R. Even, 8722
1	MS 9404	J. R. Garcia, 8725
1	MS 9405	J. M. Hruby, 8700
3	MS 9018	Central Technical Files, 8945-1
1	MS 0899	Technical Library, 9616
1	MS 9021	Classification Office, 8511 for Technical Library, MS 0899, 9616